Method for solving the gyrokinetic Poisson equation in general geometry

Z. Lin and W. W. Lee
Princeton Plasma Physics Laboratory, Princeton University, P.O. Box 451, Princeton, New Jersey 08543-0451
(Received 16 February 1995; revised manuscript received 24 May 1995)

A generalized gyrokinetic Poisson solver has been developed and implemented in gyrokinetic particle simulation of low frequency microinstabilities in magnetic fusion plasmas. This technique employs local operations in the configuration space to compute the polarization density response and automatically takes into account the background profile effects contained in the gyrokinetic Poisson equation. It is useful for the global gyrokinetic simulation of magnetized plasmas in general equilibria, where the traditional spectral method is not applicable. The numerical scheme is also most amenable to massively parallel algorithms.

PACS number(s): 02.70.−c, 52.65.Tt

I. INTRODUCTION

The gyrokinetic particle simulation technique [1–3] has been developed and extensively applied to study low-frequency microinstabilities driven by pressure gradient in magnetic fusion plasmas. The governing gyrokinetic Vlasov-Poisson system is derived by employing a two-spatial-scale expansion where the background equilibrium is assumed to be spatially uniform with respect to the fluctuation. Thus the spectral method can be utilized and the gyrokinetic Poisson equation can be solved in Fourier space. However, since the original equation is an integral equation in configuration space, the spectral results, strictly speaking, are valid only as local solutions. Therefore, the traditional spectral approach neglects the background profile effects (e.g., temperature and magnetic field) contained in the gyrokinetic Poisson equation and can treat problems only in simple geometry. In this paper, a generalized gyrokinetic Poisson solver suitable for arbitrary geometry is presented. The technique is based on the physical process of gyrophase averaging and employs local operations in configuration space to compute the polarization density response in the gyrokinetic Poisson equation. The present approach can take into account the spatial dependence of the gyrokinetic Poisson equation and is useful for nonlocal simulations as well as those associated with general geometry. This numerical scheme is also most suitable for massively parallel computing because it utilizes local operations that minimize global communications.

For simplicity, let us study the gyrokinetic Vlasov-Poisson system for simple (ion-electron) plasmas in slab geometry, which [by neglecting the nonlinear polarization effect and terms of order $\vartheta(k_\perp\rho)^4$] takes the form [1,2]

$$\frac{\partial F}{\partial t}+v_\parallel\hat{b}\cdot\frac{\partial F}{\partial \mathbf{R}}-\frac{q}{m\Omega}\frac{\partial\bar{\Phi}}{\partial\mathbf{R}}\times\hat{b}\cdot\frac{\partial F}{\partial\mathbf{R}}-\frac{q}{m}\frac{\partial\bar{\Phi}}{\partial\mathbf{R}}\cdot\hat{b}\frac{\partial F}{\partial v_\parallel}=0 \tag{1}$$

and

$$\frac{\tau}{\lambda_D^2}(\Phi-\tilde{\Phi})=4\pi e(\bar{n}_i-n_e)\ . \tag{2}$$

Here $F(\mathbf{R},\mu,v_\parallel,t)$ is the gyrocenter distribution function, which is independent of the gyrophase, $\mathbf{R}\equiv\mathbf{x}-\boldsymbol{\rho}$, $\boldsymbol{\rho}\equiv-\mathbf{v}_\perp\times\hat{\mathbf{b}}/\Omega,\Omega\equiv qB/mc$, $\hat{\mathbf{b}}\equiv\mathbf{B}/B$, $\mathbf{B}$ is the external magnetic field, $\mu\equiv v_\perp^2/2,\mathbf{v}_\parallel=v_\parallel\hat{\mathbf{b}}$, q is the signed charge, $\lambda_D\equiv\sqrt{T_e/4\pi n_0e^2}$ is the Debye length, $\tau\equiv T_e/T_i$, subscripts e and i denote species, $\Phi(\mathbf{x},t)$ is the electrostatic potential, $\bar{\Phi}$ represents the gyrophase averaged potential, and $\tilde{\Phi}$ is defined as the second gyrophase-averaged potential. Specifically,

$$\bar{\Phi}(\mathbf{R})=\frac{1}{2\pi}\int\Phi(\mathbf{x})\delta(\mathbf{x}-\mathbf{R}-\rho)d\mathbf{x}\,d\alpha\ , \tag{3}$$

where α is the gyrophase angle and $\mathbf{R}$ is held fixed in the integration, and

$$\tilde{\Phi}(\mathbf{x})=\frac{1}{2\pi}\int\bar{\Phi}(\mathbf{R})F_{Mi}(\epsilon\mathbf{R},\mu,v_\parallel)\times\delta(\mathbf{R}-\mathbf{x}+\rho)d\mathbf{R}\,d\mu\,dv_\parallel d\alpha\ , \tag{4}$$

with $\mathbf{x}$ now held fixed in the integration. In Eq. (4), F_{Mi} is assumed to be Maxwellian in $v_\perp$ and spatially slowly varying, i.e., $\epsilon\ll1$. The gyrophase-averaged ion number density is defined as

$$\bar{n}_i(\mathbf{x})=\frac{1}{2\pi n_0}\int F_i(\mathbf{R})\delta(\mathbf{R}-\mathbf{x}+\rho)d\mathbf{R}\,d\mu\,dv_\parallel d\alpha$$

and likewise n_e is the electron number density from F_e in the limit of $\rho\to0$. The background number density n_0 comes from F_e assuming $\epsilon\mathbf{x}\approx\epsilon\mathbf{R}$.

In this system, the gyrophase-averaged distribution function is a function of gyrocenter variables, i.e., $F=F(\mathbf{R},\mu,v_\parallel,t)$, while the electrostatic potential is defined in the particle or laboratory coordinates $\Phi=\Phi(\mathbf{x},t)$. Thus, to solve the gyrokinetic Vlasov-Poisson system, one has to develop a numerical algorithm to expedite the transformation. In the Fourier space, the coordinate transformation can simply be carried out by using

$$\Phi(\mathbf{x})=\sum_k \Phi_k e^{i\mathbf{k}\cdot\mathbf{x}}$$

and applying it to Eq. (3) to obtain

$$\bar{\Phi}(\mathbf{R})=\sum_k \Phi_k J_0\left[\frac{k_\perp v_\perp}{\Omega}\right] e^{i\mathbf{k}\cdot\mathbf{R}}, \tag{5}$$

where J_0 is the ordinary Bessel function, and

$$\int_0^{2\pi} \exp(\pm i\mathbf{k}\cdot\boldsymbol{\rho}) d\alpha/2\pi = J_0(k_\perp v_\perp/\Omega)$$

is utilized in this transformation. Likewise, $\tilde{\Phi}$ in Eq. (4) can be calculated in the Fourier space by assuming a spatially independent Maxwellian distribution function for the ion species and it becomes

$$\tilde{\Phi}(\mathbf{x})=\sum_k \Phi_k \Gamma_0(b) e^{i\mathbf{k}\cdot\mathbf{x}}, \tag{6}$$

where $\Gamma_0(b)=I_0(b)e^{-b}$, $b\equiv(k_\perp\rho_i)^2$, $\rho_i\equiv\sqrt{T_i/m_i}/\Omega_i$, and I_0 is the modified Bessel function. The term Γ_0 comes from

$$\Gamma_0(b)=\int J_0^2\left[\frac{k_\perp v_\perp}{\Omega}\right] F_{Mi}(\mu) d\mu, \tag{7}$$

which is the result of two gyrophase-averaging processes with respect to a Maxwellian background. Since the Debye shielding term in the gyrokinetic Poisson equation is usually neglected for the gyrokinetic particle simulations of low-frequency physics, the resulting equation is an integral equation. In simple geometry, this equation can be transformed to Fourier $\mathbf{k}$ space and solved by the fast Fourier transform (FFT) method.

The use of Fourier transform is not always practical because it involves the convolution between configuration space and velocity space through the J_0 term. For example, a better and more practical way to carry out the transformation of Eq. (3) is an averaging process of $\Phi(\mathbf{x})$ in configuration space assuming that each particle is represented by a uniformly charged ring with a radius of $\rho=v_\perp/\Omega$. Thus, integrating along the ring with sufficient accuracy, one recovers $\bar{\Phi}(\mathbf{R})$ in Eq. (3). As shown in Ref. [3], it is usually sufficient to use four points along the ring to achieve the desired accuracy for $k_\perp\rho\leq 2$ (the four-point method). As for the transformation for $\tilde{\Phi}(\mathbf{x})$ of Eq. (4) in solving Eq. (2), the spectral approach of Eq. (6) is more practical. This is because the term involving Γ_0 in Eq. (7) can be expressed as analytic functions in the $\mathbf{k}$ space. However, this approach is not applicable in general geometry, i.e., realistic tokamak equilibrium. Even in the simple case of circular cross-section toroidal geometry, the FFT approach has difficulties in implementing appropriate boundary conditions and in evaluating mode spectra. Furthermore, the gyrokinetic Poisson equation in $\mathbf{k}$ space is derived based on the two-spatial-scale assumption and one neglects the spatial dependence of the equilibrium quantities. In reality, Γ_0 should be a function of spatial coordinates when a perpendicular temperature or magnetic field gradient exists. Therefore, it is important in a realistic simulation to include the variation of temperature or magnetic field across the global simulation box. Various schemes have thus been developed to address these two problems. LeBrun and Tajima [4] employed a Padé approximation for the Γ_0 in Eq. (7) and solve the resulting gyrokinetic Poisson equation as a second-order differential equation. Li, Lee, and Parker [5] used the spectral approach in two directions, i.e., poloidal and toroidal (θ,ϕ), and utilized the Bessel function expansion in the minor radius direction for plasmas with a circular cross section. However, these approaches are not satisfactory with respect to the proper treatment of nonlocal effects and the extension to general equilibrium. Moreover, they are not applicable to a low-aspect-ratio tokamak where the poloidal magnetic field has to be included in the gyrokinetic Poisson equation.

In this paper, we present a method that enables us to carry out the transformation of $\tilde{\Phi}$ in configuration space in the same spirit as the calculation of $\bar{\Phi}$ presented in Ref. [3]. Good agreement with the FFT method is obtained in a simple test case of nonlinear simulation of η_i instability using this technique in shearless slab geometry where the FFT method is valid. In toroidal geometry, the electrostatic potential resulting from a given charge density is calculated from Eq. (2) both analytically and numerically. The results using the solver are much closer to the exact analytic solution than that of the FFT method when the same number of grid points is used. The importance of profile variation is also demonstrated in this calculation. The computational cost of the solver depends on the complexity of the geometry and represents only a few percent of the total computing time in a general toroidal equilibrium where gyrokinetic ions and adiabatic electrons are used.

The remainder of this paper is organized as follows. Section II describes the nonspectral approach for solving the gyrokinetic Poisson equation. Numerical algorithm and benchmark results for both slab and toroidal geometries are presented in Sec. III. Section IV summarizes the main findings of the present work.

II. GENERALIZED GYROKINETIC POISSON SOLVER

The key idea of the present approach is to directly calculate $\tilde{\Phi}(\mathbf{x})$ from a given $\Phi(\mathbf{x})$ in configuration space through Eqs. (3) and (4). In the particle simulation, the electrostatic potential is discretized on a grid. Therefore, $\tilde{\phi}(\mathbf{x})$ can be expressed as a linear combination of $\Phi(\mathbf{x})$'s on the grid and Eq. (2) can then be cast in a matrix form and solved by either an iteration scheme or a direct matrix inversion method. In this way, the gyrokinetic Poisson equation is solved in configuration space without transforming to $\mathbf{k}$ space.

Our starting point of analysis is Eq. (4), which relates $\tilde{\Phi}(\mathbf{x})$ on any point in configuration space to the guiding center potential $\bar{\Phi}(\mathbf{R})$ through a uniformly distributed background F_{Mi}. To calculate $\tilde{\Phi}(\mathbf{x})$ at a point $\mathbf{x}$ in configuration space, we interpret each δ function inside the integration of Eq. (4) as a uniform ring with a radius of ρ and centered at $\mathbf{x}$ (solid circle in Fig. 1). The contribution of each perpendicular velocity $v_\perp$ to $\tilde{\Phi}(\mathbf{x})$ is simply the average of the gyrophase-averaged guiding center potential $\bar{\Phi}(\mathbf{R}\equiv\mathbf{x}-\boldsymbol{\rho})$ on this ring. On the other hand,

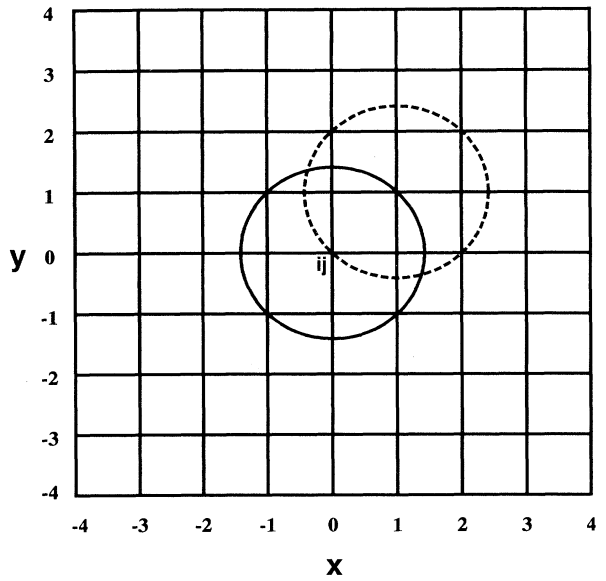

FIG. 1. Schematic procedure for the calculation of $\tilde{\phi}$ using one δ function. The length unit is ρ_i.

from Eq. (3), we known that $\bar{\Phi}(\mathbf{x}-\boldsymbol{\rho})$ of each point on this ring is evaluated by averaging the potential $\Phi(\mathbf{x})$ over another uniform ring centered at that point with the same radius (dashed circle in Fig. 1). Summing over all possible perpendicular velocities that make up the Maxwellian distribution, we thus obtain $\tilde{\Phi}(\mathbf{x})$ in terms of $\Phi(\mathbf{x})$.

With regard to the physical interpretation of this approach, let us examine how we arrive at Eq. (4). Originally, $\Phi(\mathbf{x})-\tilde{\Phi}(\mathbf{x})$ was defined as the difference between the potentials "perceived" by the particle and the guiding center [1,2]. For a known $\Phi(\mathbf{x})$, we can calculate $\bar{\Phi}(\mathbf{R})$ for each guiding center by averaging the $\Phi(\mathbf{x})$ on its uniformly charged ring. This averaged potential is then deposited back onto this ring and it represents this particle's contribution to $\tilde{\Phi}(\mathbf{x})$ on every point of this ring. Summing up the contribution from all particles, we obtained $\tilde{\Phi}(\mathbf{x})$. Alternatively, we can rewrite the original gyrokinetic Poisson equation to the form in Eq. (4) with a simplification in which the background distribution function is replaced by a spatially uniform Maxwellian in $v_\perp$. The summation process now involves an infinite number of particles with the Maxwellian distribution at every point in configuration space. However, not all particles can contribute to $\tilde{\Phi}(\mathbf{x})$. Those particles with a particular gyroradius ρ that can contribute to $\tilde{\Phi}(\mathbf{x})$ only come from a uniform ring that centers at $\mathbf{x}$ with a radius ρ. As a result, we can change the sequence of the summation process. Rather than summing over each particle contribution to $\tilde{\Phi}(\mathbf{x})$ on its uniformly charged ring, we can focus on $\tilde{\Phi}(\mathbf{x})$ at one point, first sum over all particles with a particular gyroradius that can make contribution to $\tilde{\Phi}(\mathbf{x})$, and then add up the contribution from all possible gyroradii. Thus, we recover the procedure outlined in the preceding paragraph.

To facilitate the computation, we utilize three discretization procedures. First, the averaging processes involved in the calculations of $\bar{\Phi}$ and $\tilde{\Phi}$ can be made by the average of appropriate number of equally spaced points, for example, the four-point averaging procedure, which is exact for all $k_\perp\rho \leq 2$ modes [3]. Second, note that we only need to calculate $\tilde{\Phi}$ at each grid point $\mathbf{x}_g$ instead of every point in configuration space, the resulting gyrokinetic Poisson equation is in a form of matrix equation. Finally, we can replace the Maxwellian distribution function by a sum of δ functions that are equally spaced in the perpendicular velocity space and weighted by an envelope of the normalized Maxwellian function. The exact Maxwellian distribution function is recovered in the limit of an infinite number of δ functions.

The remaining question is how many δ functions (or rings) are enough to represent the Maxwellian distribution function. We expect that only a few δ functions are needed because the Maxwellian distribution function decays exponentially for higher velocities. To verify this claim, we replace the Maxwellian by a sum of a finite number of δ functions in Eq. (4). Because the Fourier transform outlined in Sec. I is valid locally, from Eq. (6), one can see that this is equivalent to approximating Eq. (7) by

$$\Gamma_0(k_\perp^2\rho_i^2) \simeq \int J_0^2\left[\frac{k_\perp v_\perp}{\Omega}\right]\sum_j c_j\delta(\mu-\mu_j)d\mu = \sum_j c_j J_0^2\left[\frac{v_{\perp j}}{v_{\mathrm{th}\,i}}k_\perp\rho_i\right], \tag{8}$$

where c_j represents the Maxwellian envelope, $v_{\perp j}$ is the perpendicular velocity of the jth ring, and $v_{\mathrm{th}i} \equiv \sqrt{T_i/m_i}$ is the ion thermal velocity. This approximation becomes exact when an infinite number of δ functions is used. Practically, Eq. (8) is realized by choosing a finite number of c's and $v_\perp$'s such that the function ϵ is minimized,

$$\epsilon(c,v_\perp) = \int_0^{x_{\mathrm{mas}}}\left[\Gamma_0(x^2)-\sum_j c_j J_0^2(xv_{\perp_j}/v_{\mathrm{th}i})\right]^2 dx\ , \tag{9}$$

where $x \equiv k_\perp\rho_i$ and $x_{\max}$ is associated with the maximum wave number of interest. In the gyrokinetic particle simulation, $k_\perp$ varies only in the range of $0 < k_\perp\rho_i < \pi\rho_i/\Delta x$, where Δx is the grid spacing, and the mode amplitude is usually small for the $k_\perp\rho_i > 1$ modes for the low-frequency microinstabilities. The dominate fluctuations in this case are usually in the range $0.1 < k_\perp\rho_i < 0.5$. Therefore, it is imperative that this discretization is accurate in the long-wavelength limit. For example, in Eq. (9), we match the first two terms of the small parameter expansion for the Bessel function, i.e., $J_0(xv_{\perp j}/v_{\mathrm{th}i}) \sim 1-(xv_{\perp j}/v_{\mathrm{th}i})^2/4+\cdots$ and the Padé approximation of $\Gamma_0(x^2) \sim 1/(1+x^2) \sim 1-x^2+\cdots$, and arrive at the constraints

$$\sum_j c_j = 1$$

and

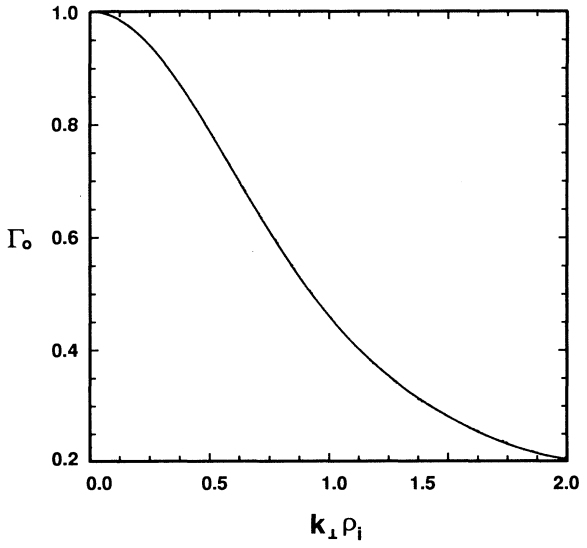

FIG. 2. Approximate Γ_0, calculated using three δ functions (dotted line), compared with the exact Γ_0 (solid line).

$$\sum_j \tfrac{1}{2} c_j (v_{\perp j}/v_{thi})^2 = 1 \ .$$

These constraints reduce the number of free parameters of c's and $v_\perp$'s by 2.

To calculate the optimal c's and $v_\perp$'s, a set of random numbers is generated for these quantities and its corresponding ϵ given by Eq. (9) is calculated. Then, each set of c's and $v_\perp$'s with the minimum ϵ is identified for any chosen number of δ functions. To reduce the computational cost, it is desirable to use as few δ functions (rings) as possible. It turns out that one ring with $c=1$ and $v_\perp/v_{thi}=\sqrt{2}$ give reasonably good agreement for $k_\perp \rho_i \leq 0.5$. Two rings with $c=(0.7194, 0.2806)$ and $v_\perp/v_{thi}=(0.9130, 2.2339)$ can fit Eq. (8) very well (less than 1% error) up to $k_\perp \rho_i \simeq 1.5$. Practically, we use three rings with $c=(0.3583, 0.5004, 0.1413)$ and $v_\perp/v_{thi}=(0.5443, 1.4142, 2.5138)$, which works very well over the range $0 < k_\perp \rho_i \leq 2$. In Fig. 2 the approximate Γ_0 (dashed line) using these three δ functions is compared with the exact Γ_0 (solid line). It is obvious that this approximate solution is almost exact. By contrast, Fig. 3 shows a much larger error (9%) for the Padé approximation (dashed line), which is extensively used in both analytical and numerical studies. The error in Γ_0 will lead to incorrect linear growth rates and nonlinear saturation amplitudes.

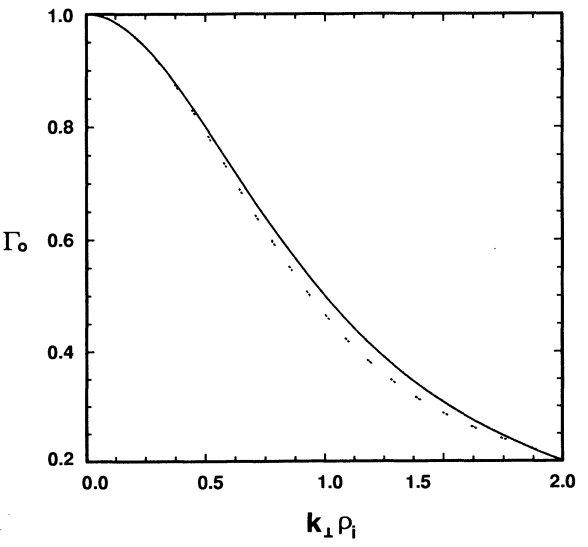

FIG. 3. Padé approximation of Γ_0 (dotted line) compared with the exact Γ_0 (solid line).

III. NUMERICAL IMPLEMENTATION AND TEST CASE RESULTS

A. Slab geometry

To illustrate the numerical procedure, let us use only one ring (one δ function) with $c=1$ and $v_\perp=\sqrt{2}v_{thi}$ to calculate $\tilde{\Phi}(x)$ in slab geometry with uniform electron temperature and $\tau=1$. Throughout this paper, gyrokinetic normalization is used, i.e., $B_0=m_i=T_e=e=1$, where B_0 and T_e are the quantities at a reference point. Thus the length unit is $\rho_s=\sqrt{\tau}\rho_i$, the time is Ω_i^{-1}, and the electrostatic potential is T_e/e. The two four-point averaging processes are shown in Fig. 1, where the grid spacing is chosen to be equal to the ion thermal gyroradius ρ_i. Here $\tilde{\phi}_{i,j}$ at a grid point (i,j) is the average of $\bar{\Phi}(\mathbf{R})$ on a ring (solid) that is centered at this point with a radius of $\rho=\sqrt{2}\rho_i$. Thus $\tilde{\Phi}_{i,j}$ is simply the four-point average of $\bar{\Phi}(\mathbf{R})_{(i\pm1,j\pm1)}$. The value of $\bar{\Phi}(\mathbf{R})$ at each of these points $(i\pm1, j\pm1)$, in turn, is calculated by averaging Φ on another ring (dashed) centered at that point with the same radius. This second averaging process is also carried out by the four-point averaging scheme. The whole process gives

$$\tilde{\Phi}_{i,j} = \tfrac{1}{16}(4\Phi_{i,j} + 2\Phi_{i\pm2,j} + 2\Phi_{i,j\pm2} + \Phi_{i\pm2,j\pm2}) \ ,$$

where $\Phi_{i,j}$ is the potential at grid point (i,j). This expression of $\tilde{\Phi}$ is put back into Eq. (2) and the resulting gyrokinetic Poisson equation is in a matrix form. It can then be solved either by an interation scheme or by a direct matrix inversion operation. Since Γ_0 is always smaller than 1 and only varies in a limited range, the convergence for the iteration scheme is guaranteed and is actually quite fast. When the electron is adiabatic and $\tau=1$, we have found that sufficient accuracy can be achieved by at most five iterations.

In more general cases where the ring does not pass through the grid points, the potential on the ring can be calculated by the linear interpolation of potential from the nearby grid points. When a relatively large perpendicular velocity is used, eight-point averaging instead of four-point averaging may be used to achieve desired accuracy. In the rest of this paper, as for the purpose of gyrokinetic simulations of microinstabilities in magnet-

ized plasmas, the three-ring method in velocity space is used along with the four-point averaging procedure in configuration space.

The proper boundary conditions for Eq. (2) can be easily implemented in this process. For example, by extending the grid array beyond the simulation boundary, one can assign the appropriate values for the Φ's outside the boundary by using those inside the boundary to account for the usual periodic or perfect conducting boundary conditions. Only those $\bar{\Phi}$'s inside or on the boundary are needed in the calculation.

In the usual FFT approach, numerical filter of the form $f_{\mathbf{k}}=\exp[-(\mathbf{s}\cdot\mathbf{k})^2]$ is usually applied in $\mathbf{k}$ space, i.e., $f_{\mathbf{k}}\Phi_{\mathbf{k}}\rightarrow\Phi_{\mathbf{k}}$, to cut off the fluctuations for the high $\mathbf{k}$ modes in order to reduce the simulation noise. Here $\mathbf{s}$ represents the lower bound of the wavelength of interest. Similar filters can be constructed by numerical smoothing in configuration space. To simplify the analysis, let us consider a one-dimensional uniform grid with a spacing of Δx. We can cut off short-wavelength modes by replacing the potential at each grid point with a weighted average of potential at several adjacent grid points. Let us assume

$$\Phi(x)=\sum_n \alpha_n \Phi'(x\pm n\Delta x)\ ,$$

where α is the weighted factor and $\Phi(x)$ and $\Phi'(x')$ are the potentials after and before the numerical smoothing, respectively. Then, from the convolution theorem, this configuration space smoothing is equivalent to applying the following form factor in the $\mathbf{k}$ space:

$$f_k=\sum_n \alpha_n \cos(kn\Delta x)\ ,$$

where α_n's are set by choosing a desired form factor of filtering. For example, simple smoothing with $\Phi_{i,j}=\frac{1}{4}(2\Phi'_{i,j}+\Phi'_{i\pm1,j})$ gives a numerical filtering of the form $f_k=\cos^2(k\Delta x/2)$, which is similar to $f_k=\exp[-(sk)^2]$ with $s=\Delta x/2$.

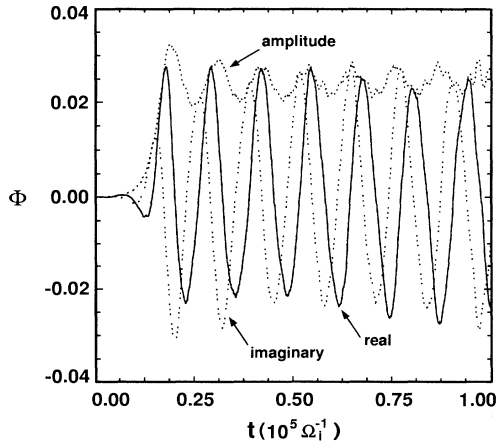

FIG. 4. Mode history of the electrostatic potential using the FFT method. The time unit is Ω_i^{-1} and the potential unit is T_e/e.

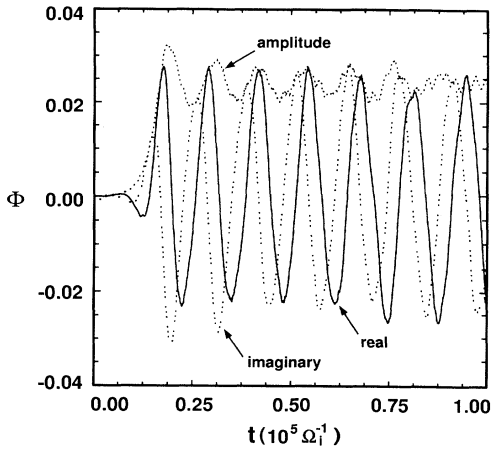

FIG. 5. Mode history of the electrostatic potential using the generalized Poisson solver. The time unit is Ω_i^{-1} and the potential unit is T_e/e.

To test the Poisson solver, nonlinear simulation of ion temperature gradient instability (η_i mode) with $k_\perp\rho_i\simeq0.4$ has been carried out in a shearless slab with adiabatic electron response [6]. The background temperature variation has been neglected so that the FFT method is valid. The present Poisson solver uses three rings and four iterations. The mode history of the electrostatic potential using the FFT and the present iteration scheme is plotted in Figs. 4 and 5, respectively. It is shown that the present scheme gives results in excellent agreement with those from the FFT method, which is valid for slab geometry.

B. Toroidal geometry

In this subsection we compare the results of the present scheme with the exact solution of Li, Lee, and Parker [5] in toroidal geometry. The potential in this case can be expressed as the Bessel-Fourier series in terms of the toroidal coordinates (r,θ,ϕ),

$$\Phi(\mathbf{x})\equiv\Phi(r,\theta,\phi)=\sum_{l,m,n,}\Phi_{lmn}J_m\left[\frac{\alpha_{ml}r}{a}\right]e^{i(m\theta+n\phi)},$$

where r, θ, and ϕ are in the minor radius, the poloidal direction, and the toroidal direction, respectively, α_{ml} is the lth zero of the Bessel function J_m, and a is the minor radius. This set of trial functions satisfies the regularity condition at $r=0$ and the boundary condition of $\Phi(r=a)=0$. Assuming a pure toroidal magnetic field and a circular cross section, one can carry out the gyrophase-averaging procedure to obtain

$$\bar{\Phi}(\mathbf{R})\equiv\bar{\Phi}(r_0,\theta_0,\phi)$$
$$=\sum_{l,m,n}^{\infty}\Phi_{lmn}J_0\left[\frac{\alpha_{ml}\rho_i}{a}\right]J_m\left[\frac{\alpha_{ml}r_0}{a}\right]e^{i(m\theta_0+n\phi)},$$

where (r,θ_0,ϕ) is the guiding center coordinates in toroidal geometry. Again assuming a Maxwellian equilibrium, the second gyrophase-averaged potential $\tilde{\Phi}$ can be expressed as

$$\tilde{\Phi}(\mathbf{x})=\sum_{l,m,n}^{\infty}\Gamma_0\left[\frac{\alpha_{ml}^2\rho_i^2}{a^2}\right]\Phi_{lmn}J_m\left[\frac{\alpha_{ml}r}{a}\right]e^{i(m\theta+n\phi)}.$$

Utilizing this relation, the gyrokinetic Poisson equation can be expressed in Bessel-Fourier space as a matrix equation

$$\frac{\tau}{\lambda_D^2}\sum_{l,m,n}\Phi_{lmn}\left[1-\Gamma_0\left[\frac{\alpha_{ml}^2\rho_i^2}{a^2}\right]\right]\times J_m\left[\frac{\alpha_{ml}r}{a}\right]e^{i(m\theta+n\phi)}=-4\pi e(\bar{n}_i-n_e)\,. \quad (10)$$

This equation is coupled in the θ and r directions due to the dependence of ρ_i on θ and r.

The relative accuracy of the Poisson solver with the FFT method in toroidal geometry can now be assessed. For this purpose we assume that the magnetic field and the background temperature are uniform in space. Thus ρ_i is independent of r, θ, and ϕ and the gyrokinetic Poisson equation is decoupled for different l, m, and n modes. Given charge density as the sum of a finite series of the Bessel-Fourier trial functions, the potential can be obtained analytically using Eq. (10). This result can then be compared with those numerically calculated from the same charge density by the present generalized Poisson solver and the FFT method, respectively. Figure 6 depicts the potential as a function of r calculated by analytical solution (solid line), the generalized Poisson solver (dotted line), and the FFT method (dashed line), respectively. It is shown that the Poisson solver is more accurate than the FFT method, although the same number of grid points is used for both approaches. The difference is especially obvious near the edge ($r=a$). In this comparison, a single toroidal mode (uniform) is used and the perpendicular power spectra for the potential with $k_\theta\rho_i\simeq 0.4$ are shown in Figs. 7 and 8. These spectra are similar to those in the toroidal η_i instability simulation [7]. In the calculation using the Poisson solver, the r-θ plane is divided into equal area cells (uniform grid spacing in r^2-θ) with an area element of $\Delta r^2\Delta\theta=\rho_i^2$. The number of grid points in the r and θ directions is arranged in such a way that each direction has the same resolution near the half minor radius where the most interesting physics usually takes place. The FFT method uses the usual x-y coordinate with the grids spacing of $\Delta x=\Delta y=\rho_i$. When more grid points are used, the results for both methods approach the exact solution.

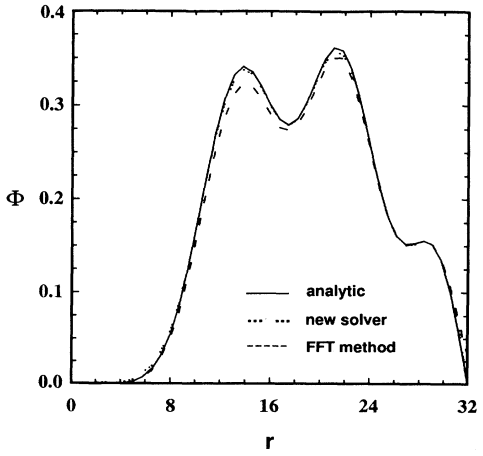

FIG. 6. Electrostatic potential (in arbitrary units) at $\theta=0$ vs minor radius (in unit of ρ_i) calculated by the analytic method (solid line), the FFT method (dashed line), and the generalized Poisson solver (dotted line).

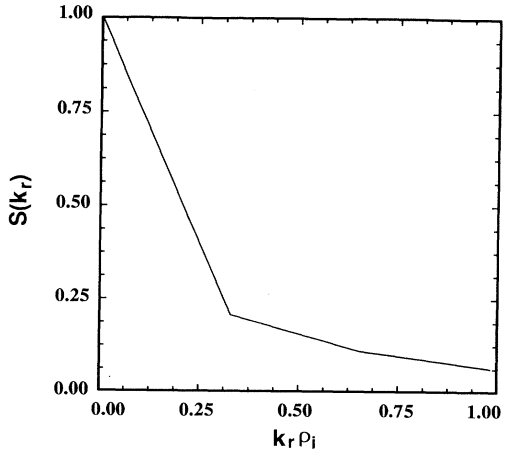

FIG. 7. k_r spectrum (in arbitrary units) of the potential in Fig. 6.

Next, we study the modification to the potential due to the background temperature variation. Assuming a temperature profile as shown in Fig. 9, the potential calculat-

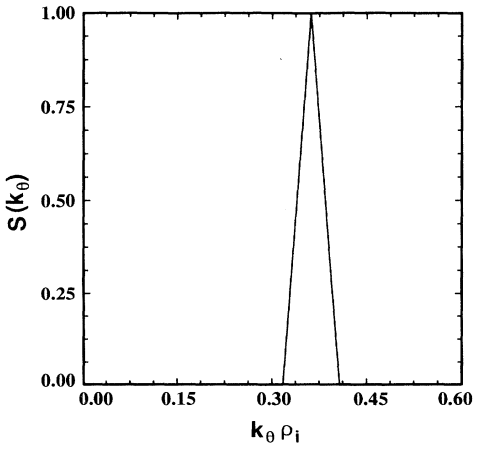

FIG. 8. k_θ spectrum (in arbitrary units) of the potential in Fig. 6.

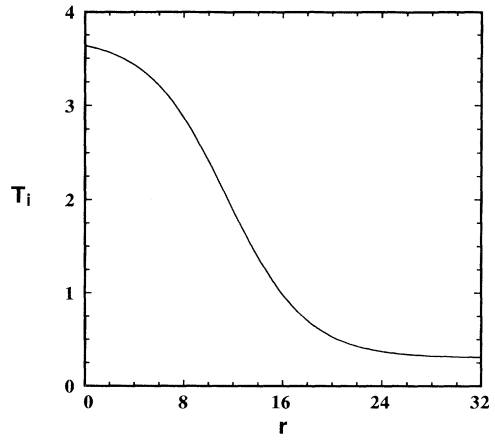

FIG. 9. Model for the temperature profile. The length unit is ρ_i.

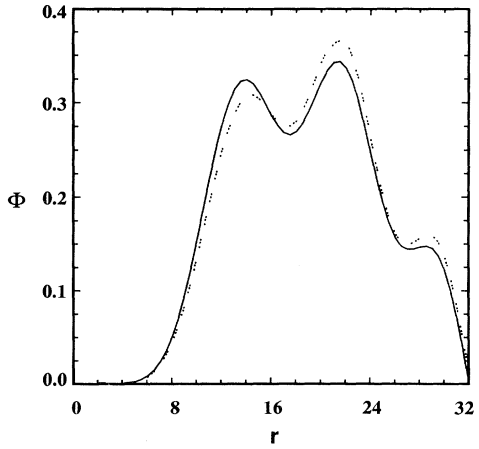

FIG. 10. Electrostatic potential (in arbitrary units) at $\theta=0$ vs minor radius (in units of ρ_i) with the temperature profile effect retained (dotted line). The solid line represents the potential calculated without taking into account profile effect.

ed by the generalized Poisson solver taking into account the profile effect is shown as a dotted line in Fig. 10. The solid line in the same figure represents the analytical solution calculated from Eq. (10) without taking into account the background profile effects. The same charge density that produces the potential in Fig. 6 is used for this calculation. Although the modification is modest in this particular example, it can accumulate for each time step in the simulation and may modify linear eigenmodes and nonlinear steady-state results.

The computational cost of the Poisson solver depends on the complexity of the geometry, but it can be made quite efficient. In term of the Cray-C90 vector computer single CPU time, this solver is faster than the FFT method in a shearless slab with the adiabatic electrons and a uniform background temperature. In toroidal geometry with 10^6 grid points, the present solver takes 0.5 μs per grid point per iteration (4 μs per time step assuming four iterations in both predictor step and corrector step) when the electrons are assumed to be adiabatic and the background temperature and magnetic field are nonuniform. Since it takes 8 μs per particle per time step for the particle pusher and usually more than one particle per grid point is used in the three-dimensional simulations, the Poisson solver represents only a small portion of the total computational cost of the simulation. Furthermore, the present solver scales as the number of grid points in terms of the CPU time, while the usual spectral approach scales as N ln$N$ for N grid points. The actual relative cost of the present Poisson solver decreases with the increasing simulation system size because of the better vectorization.

IV. CONCLUSION

A non-FFT gyrokinetic Poisson solver has been developed and implemented in the gyrokinetic particle simulation of low-frequency microinstabilities in magnetized plasmas with general equilibrium. The technique can also take into account the spatial dependence of the equilibrium profile in the gyrokinetic Poisson equation and is general enough to treat the non-Maxwellian background distribution. This approach employs local operations and therefore is useful for the global simulation in general geometry on massively parallel computers.

ACKNOWLEDGMENTS

The authors would like to thank Dr. S. E. Parker, Dr. J. C. Cummings, and Dr. J. V. W. Reynders for useful discussions. This work was supported by the U.S. Department of Energy under Contract No. DE-AC02-76-CHO3073.

[1] W. W. Lee, Phys. Fluids **26**, 556 (1983).
[2] D. H. E. Dubin, J. A. Krommes, C. Oberman, and W. W. Lee, Phys. Fluids **26**, 3524 (1983).
[3] W. W. Lee, J. Comput. Phys. **72**, 243 (1987).
[4] M. J. LeBrun and T. Tajima, Bull. Am. Phys. Soc. **39**, 1533 (1994).
[5] J. Li, W. W. Lee, and S. E. Parker (unpublished).
[6] W. W. Lee and W. M. Tang, Phys. Fluids **31**, 612 (1988).
[7] S. E. Parker, W. W. Lee, and R. A. Santoro, Phys. Rev. Lett. **71**, 2042 (1993).